Friction **11**(7): 1150–1164 (2023)
https://doi.org/10.1007/s40544-022-0632-7
ISSN 2223-7690
CN 10-1237/TH
RESEARCH ARTICLE

Study on the microcosmic superlubricity mechanism of PVPA affected by metal cations

Hongyun CAI[1], Caixia ZHANG[1,2,*], Fuping LI[1,2], Mengmeng LIU[1], Tao ZHANG[1,2], Hongyan CHU[1,2], Zhifeng LIU[2,3,*]

[1] *Institute of Advanced Manufacturing and Intelligent Technology, Faculty of Materials and Manufacturing, Beijing University of Technology, Beijing 100124, China*

[2] *Machinery Industry Key Laboratory of Heavy Machine Tool Digital Design and Testing Technology, Faculty of Materials and Manufacturing, Beijing University of Technology, Beijing 100124, China*

[3] *Key Laboratory of CNC Equipment Reliability, Ministry of Education, School of Mechanical and Aerospace Engineering, Jilin University, Changchun 130025, China*

Received: 29 March 2021 / Revised: 13 July 2021 / Accepted: 05 April 2022

Abstract: Hydrophilic polymer coatings on artificial implants generate excellent tribological properties. The friction properties of polymer coatings are affected by salt ion factors. Herein, the atomic force microscopy (AFM) was used to show that the superlubricity was achieved between poly(vinylphosphonic acid) (PVPA)-modified Ti6Al4V and polystyrene (PS) microsphere probe lubricated with monovalent salt solutions (LiCl, NaCl, KCl, and CsCl). Considering that adhesion is an important cause of friction changes, the AFM was further utilized to obtain adhesion between friction pairs in different salt solutions. The results indicated that the larger the cation radius in the lubricant, the smaller the adhesion, and the lower the friction coefficient of the PVPA coating. The electrostatic interaction between the PVPA and one-valence cations in lubricants was analyzed by the molecular dynamics (MD) simulation as it was found to be the main influencing factor of the adhesion. Combined analysis results of friction and adhesion indicated that by adjusting the size of cation radius in lubricant, the adhesion between the tribo-pairs can be changed, and eventually the magnitude of friction can be affected. This study opens up a new avenue for analyzing the friction characteristics of hydrophilic polymer coatings from the perspective of intermolecular forces.

Keywords: atomic force microscopy (AFM); superlubricity; poly(vinylphosphonic acid) (PVPA); cation; adhesion; molecular dynamics (MD) simulation

1 Introduction

The modification of the surface of biological materials with hydrophilic polymers can effectively reduce the friction between the surface and the interface. Among these modification processes, the variation in the adhesion properties of the hydrophilic polymer surface plays a vital role in the regulation of friction [1–5]. Poly(vinylphosphonic acid) (PVPA) is a type of hydrophilic polymer possessing excellent characteristics including good biocompatibility, hydrophilicity, and coating stability, and thus it is extensively employed in the surface modification of titanium alloys for lubrication of joints for reducing the friction [6–10]. Moreover, PVPA coatings exhibit different friction coefficients in different salt solutions, indicating that the compatibility between PVPA coatings and lubricants regulates its superlubricity, which may be related to its surface characteristics [11–15].

Considering the application of biological materials with hydrophilic polymer coatings in the human body to improve the surface characteristics of artificial

* Corresponding authors: Caixia ZHANG, E-mail: zhang-cx15@bjut.edu.cn; Zhifeng LIU, E-mail: lzf@bjut.edu.cn

implants, the surface of the hydrophilic polymer coating inevitably comes in contact with salt ions in body fluids [16, 17]. Therefore, the interaction between the salt ions and the surface of biological materials has attracted significant research attention [18–20]. Moreover, the atomic force microscopy (AFM) measurement technology with ultra-micro-scale ultra-high resolution has emerged as a powerful tool to obtain the nanostructural details and biomechanical properties of biological samples including biomolecules and cells. The AFM can accurately reflect the properties of the surface and interface on the nano-scale, and has become an important method for direct measurement of (sub)micron-scale friction and adhesion force [21–27]. Traditional AFM probe consists of a conical tip, which is used to obtain the force curve to analyze the data [28, 29]. However, in traditional AFM probes, the tip always exerts a mechanical load on the sample, which may damage the sample surface. Therefore, to overcome these issues, the colloidal probe technology was introduced in 1991 [30]. At present, the most widely used technique involves the use of silica microspheres and polymer microspheres made of polystyrene (PS) or polyethylene [31–33] to study the adhesion characteristics between the surfaces. Moreover, the development of AFM ball needle technology provides more favorable support for systematic investigation of the factors influencing the tribological properties. According to the literature, the friction and adhesion between the two surfaces where friction occurs is affected by several factors. For example, the microstructure, roughness, and surface charge of the polymer can affect the frictional properties of the polymer at its surface [34–36]. Some scholars pointed out the existence of a strong correlation between friction and adhesion, indicating that depending on whether there is adhesion force constituting the normal force between the surface and interface, a higher or lower friction coefficient is obtained between the tribo-pairs [37–40]. When using the AFM colloidal probe to study the specific effect of adhesion on friction, some studies have also found that the adhesion between spherical probe and polymer coating is attributed to the contribution of van der Waals interaction, electrostatic interaction, hydrogen bond, etc. [41–43]. The above-mentioned studies provide numerous new ideas for further investigation of the friction properties of polymer under microscopic conditions.

Noteworthy, the surface friction and adhesion of the polymer coating is not only affected by the intermolecular interaction force, but also depends on its own specific structural characteristics [44]. In the salt solution, the molecular chain and the movement process of salt ions and water molecules are mainly involved; therefore, it is difficult to measure them by experimental means [45, 46]. As a result, molecular simulation has become an effective method to study polymer microstructure and intermolecular interaction process. Owing to the advantages of the molecular dynamics (MD) simulation technology, many studies at the global scale have realized the integration of calculation method and experimental method to obtain specific parameters and scale [47, 48]. Under the condition of water lubrication or salt solution lubrication, the simulation model of tribo-pairs can be used to analyze the force between the probe tip and the polymer surface [49]. It is revealed that the repulsion or attraction between the two is the main reason for the low friction coefficient [50, 51]. It can not only explain the friction mechanism from the perspective of molecular motion, but also predict some surface and interfacial properties [52, 53].

To the best of our knowledge, the characteristics of PVPA molecular chain structure and other characteristics of metal cations in salt solutions from the perspective of the forces between molecules and atoms have rarely been reported. In this study, the friction characteristics of polymer molecular chains on micro and nano scales were comprehensively studied by integrating experiments and simulations, as well as the influence mechanism on the frictional properties of molecular chains due to different interactions among the molecules was investigated. The electrostatic interaction between polymer molecular chains and metal cations in different salt solutions may explain why the friction and adhesion of hydrophilic phosphonic acid polymers decrease with the increase of metal cation radius. This research not only provides a theoretical basis for further understanding the microscopic friction characteristic of phosphonic acid polymers from a molecular perspective, but also offers important theoretical guiding significance for similar research.

2 Materials and methods

2.1 Materials

PVPA (97%) was supplied by Sigma-Aldrich, USA. LiCl, NaCl, KCl, and CsCl were purchased from J&K Chemicals (Beijing, China). The average molecular weight of the PVPA is 24,817 g/mol. Ti6Al4V (100 mm × 100 mm) foils with a thickness of 1 mm were supplied by Goodfellow Inc. (Cambridge, UK). These foils were then polished with a polishing slurry (Southwest Jiaotong University, Chengdu, China) to achieve flat and smooth surfaces (Ra = 2 nm). All the reagents mentioned above were used as received without any further purification.

2.2 Preparation of PVPA coatings

First, the polished Ti6Al4V sheet was placed in a poly(tetrafluoroethylene) mold. Second, the prepared PVPA aqueous solution (1 mg/mL) was dropped onto the Ti6Al4V sheet until the entire mold was completely filled. Then, after evaporating the solvent in the air atmosphere at a temperature of 50 °C for 30 h, a PVPA coating was formed on the surface of the Ti6Al4V substrate. Finally, the Ti6Al4V covered with PVPA coating was placed in an oven at 240 °C for an annealing time of 6 h. After the above-mentioned steps, a stable PVPA coating on the Ti6Al4V chip was successfully obtained.

2.3 AFM for the evaluation of friction and adhesion characteristics

For all the experiments, AFM technique (Asylum Research MFP-3D SA microscope, Santa Barbara, USA) was used to test the friction and adhesion behaviors of PVPA coatings. The force curve mode was adopted during the submerged experiment. The temperature during the friction and adhesion experiment was controlled at 37 °C in order to reflect the body temperature.

The friction circuit is composed of lateral trace and lateral retrace scans, and the friction circuit curve of each sample was obtained by the AFM. Owing to the large curvature of the ball, the traditional grating pitch was too short, and the slope length was also short; therefore, effective plane and slope data could not be obtained. Thus, in the experiment, a new calibration grating was fabricated on the surface of the silicon wafer by the focused ion beam (FIB) etching method introduced by the Scanning Electron Microscope Laboratory of Tsinghua University, Beijing, China. The size and morphology of the prepared calibration grating were obtained by the scanning electron microscopy (SEM; Quanta200, FEI Company, Hillsboro, USA), as shown in Fig. 1. The FIB-etched grating was used to calibrate the lateral force of the AFM probe, and the friction voltage signal (half the difference between LateralTrace and LateralRetrace) obtained in the experiment was converted into frictional force. The slope between the frictional force and the normal force provides the friction coefficient.

2.4 SEM observation of the prepared PS microsphere probe morphology

In this study, the Quanta200 type scanning electron microscope from FEI Company, Hillsboro, USA, was used, which mainly includes the following three working modes: high vacuum, low vacuum, and

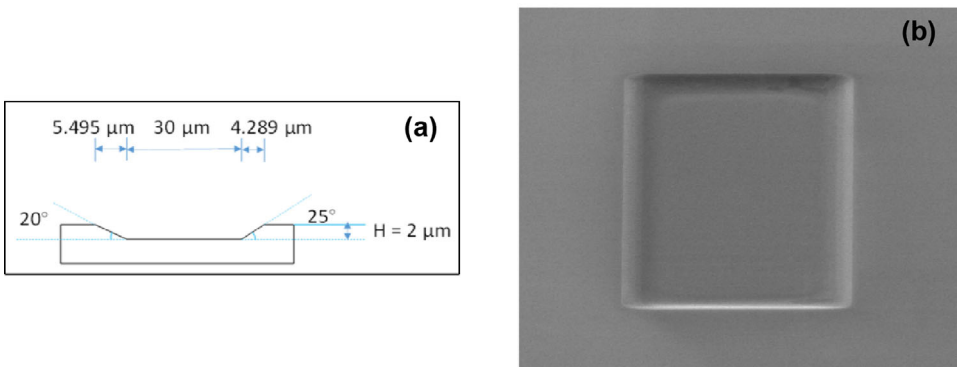

Fig. 1 Calibration grating after the FIB etching: (a) specific size of the grating; (b) SEM image of the calibration grating.

environment. In this study, it was mainly used for the microscopic morphology measurement of calibration grating and PS ball probes.

2.5 Simulation

All the simulations were performed by using BIOVIA Materials Studio software based on the MD methods. This research utilizes PVPA polymer materials as the research object. In order to study the changing behavior of PVPA in different salt solutions, the amorphous cell module was used. Herein, a three-dimensional (3D) periodic structure composed of water molecules, inorganic salt ions, polymeric molecular chains, and built cells was fabricated according to the density, number of chains, and degree of polymerization.

Moreover, another module named Forcite in BIOVIA Materials Studio was used for further investigations. This module aided in calculating the changes in internal properties of PVPA after interacting with water molecules and inorganic salt ions. In this study, all the force fields used corresponded to COMPASS force fields.

2.5.1 Structural formula of vinyl phosphonic acid

The PVPA chain is composed of the polymerized vinylphosphonic acid units. First, a new 3D Atomistic Document was opened in which a structural sketch was drawn. Then, a vinyl phosphonic acid unit was drawn in the corresponding file to optimize its structure (Fig. 2).

2.5.2 Consistency of simulation and experimental parameters

In this study, the periodic table of the new 3D Atomistic Document module in the Materials Studio software was used to build various atomic models. The default charge was 0, and it did not contain any charged valence states. Therefore, in order to analyze the influence of the adsorption of different inorganic salt ions on the PVPA molecular chain, allocation of the charge to the metal atoms mentioned above was extremely important. In order to meet the needs of force field distribution, this study adopted a manual charge distribution method to change the above-mentioned metal atoms into the charged valence state required in the following study.

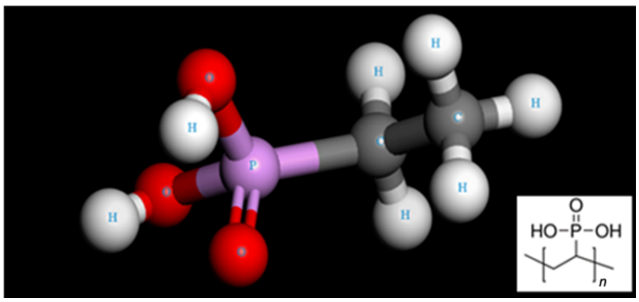

Fig. 2 Optimized vinyl phosphonic acid unit.

Then monovalent cations (Li^+, Na^+, K^+, and Cs^+), divalent cations (Mg^{2+} and Ca^{2+}), and anions (Cl^-) were drawn in different tasks. Divalent cations were used as a control group to verify relevant conclusions. Considering that the salt solution concentration in the experiment was 0.5 mol/L, it was calculated that 1,000 water molecules corresponded to 9 anions (the cations are Li^+, Na^+, K^+, and Cs^+) and 18 anions (the cations are Mg^{2+} and Ca^{2+}). Next, modeling was carried out based on the above-mentioned accurate values (Table 1).

2.5.3 Model establishment and optimization of PVPA molecular chain

The Build module in the Materials Studio software was used to construct the PVPA polymer molecular chain with the chain length of 30, using the vinyl phosphonic acid unit. The structure and energy of the initial PVPA molecular chain model were not in the best state, and would be further optimized. Figure 3 demonstrates that after energy and structure optimization, the energy of PVPA's molecular chain was significantly reduced, resulting in the lowest energy configuration.

Table 1 Specific parameters of unit cells in different inorganic salt solutions.

Type of salt solution	Number of molecular chains	Number of water molecules	Number of cations	Number of anions
LiCl	1	1,000	9	9
NaCl	1	1,000	9	9
KCl	1	1,000	9	9
CsCl	1	1,000	9	9
$MgCl_2$	1	1,000	9	18
$CaCl_2$	1	1,000	9	18

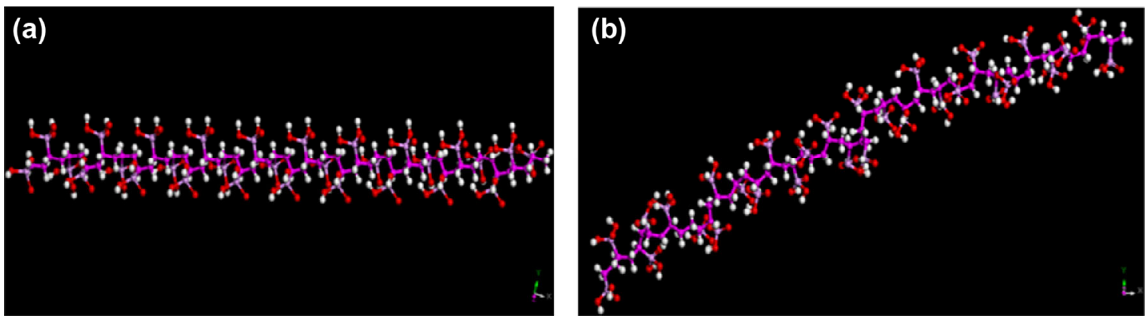

Fig. 3 PVPA molecular chain with 30 repeating units: (a) before optimization; (b) after optimization.

3 Results and discussion

3.1 Effects of metal cations in different salt solutions on the friction characteristics of PVPA molecular chains

The friction experiments were carried out using an atomic force microscope, under the temperature of 37 °C, the scanning angle of 90°, and the scanning speed of 0.5 Hz. The PVPA-modified Ti6Al4V sheet and PS microspheres were used as tribo-pair materials for conducting microscopic experiments. LiCl, NaCl, KCl, and CsCl were used as lubricants for friction experiments. The friction of all samples was measured under different loads between 0 and 600 nN applied using the AFM probe.

When measuring the friction force, the probe is very sensitive to the measuring force, and thus the TL-CONT rectangular cantilever (without needle tip) was selected, and microspheres with diameter of 20 μm were used to obtain a more approximate planar contact effect. In the experiment, the PS microspheres were glued to the tip of the cantilever beam with the AB glue to fix together the microspheres and the cantilever beam. Figure 4 exhibits the SEM morphology of the prepared PS ball probe, clearly indicating the absence of defects such as glue overflow and glue leakage around the prepared microsphere probe, which fully meets the experimental requirements.

During the submerged experiment of the atomic force microscope, the friction forces between PVPA-modified Ti6Al4V and PS ball in different salt solutions (LiCl, NaCl, KCl, and CsCl) were measured. By linearly fitting the measurement data, the corresponding friction force–normal force curve was obtained, as shown in Fig. 5.

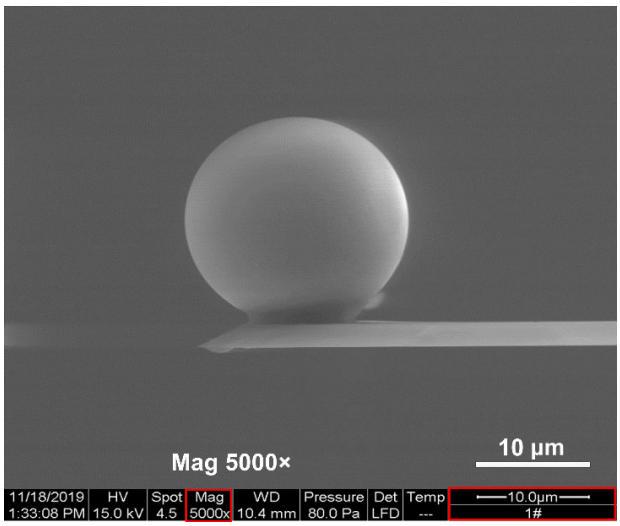

Fig. 4 SEM image of PS beads: 5000× magnification.

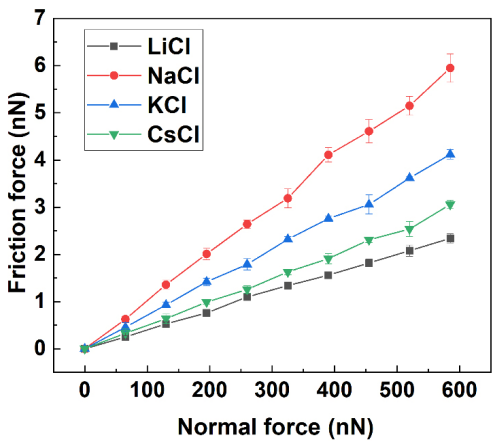

Fig. 5 Friction forces between PVPA-modified Ti6Al4V and PS ball in different salt solutions.

Figure 5 illustrates that the load and friction exhibit a good linear relationship, and the friction coefficient can be obtained by fitting the slope. When LiCl, NaCl, KCl, and CsCl solutions are used as lubricants, the friction coefficients of the PVPA surface are

0.004±0.001, 0.010±0.003, 0.007±0.002, and 0.005±0.002, respectively. Noteworthy, the friction coefficient reflects the friction characteristics of the sample in a liquid environment, that is, the friction force increases linearly with the increase of positive pressure. Moreover, the friction coefficient of the sample in a liquid environment can reach superlubricity. This is attributed to the fact that the tribo-pair is in a boundary lubrication state in a liquid environment, and the surface of the PVPA coating adsorbs water molecules in the solution and forms a very thin water molecule lubricating film. The existence of this thin lubricating film effectively reduces friction.

Moreover, comparative analysis indicates that for the monovalent cation system, with the increase in the radius of the metal cation in the salt solution (Na^+ < K^+ < Cs^+), the friction coefficient of PVPA surface decreases. However, the friction coefficient of PVPA coating in LiCl is the smallest, which is lower than those in NaCl, KCl, and CsCl. The appearance of frictional force on the polymeric surface is often considered to be the result of a variety of factors on the surface and interface, including surface adhesion characteristics, surface charge, and so on. Therefore, with the objective of comprehensively explaining the specific effects of metal cations in different salt solutions on the surface friction characteristics of PVPA, it is necessary to evaluate the changes in the adhesion between PVPA-modified Ti6Al4V and PS ball.

3.2 Adhesion characteristics of PVPA surface lubricated based on different salt solutions

The interaction between the salt ions in the lubricant and the polymer molecular chains leads to the change in the properties of the polymer molecules, thereby affecting the friction results. Importantly, the difference in adhesion characteristic between PVPA-modified Ti6Al4V and PS ball in different lubricants is an important factor that cannot be ignored. In this study, the adhesion between PVPA-modified Ti6Al4V and PS ball in different salt solutions was obtained by submerged experiments performed through AFM.

During the experiment, the AFM output is the corresponding voltage signal and not the direct force signal. The adhesion F_{af} can be obtained by using Eq. (1):

$$F_{af} = k_c \times \mathrm{InvOLS} \times d \tag{1}$$

where k_c (nN/nm) is the normal stiffness, and InvOLS (nm/V) is the sensitivity term, which is responsible for converting force–displacement signals into force–voltage signals. By drawing a force curve on the substrate with the probe, the relationship between the elongation (nm) of the piezoelectric ceramic and the deformation (V) of the cantilever beam was attained, and the corresponding sensitivity value was obtained by calculating the slope. Further, d denotes the deformation value (V) of the cantilever system at the front end of the PS microsphere probe, which is generally obtained through performing specific experiments.

In order to obtain an accurate adhesion value, the entire cantilever beam system was calibrated to obtain an accurate k_c of the cantilever beam system. In this study, the thermal noise method was used to calibrate k_c (nN/nm). The probe was approximated as a harmonic oscillator, and the k_c of the cantilever beam can be obtained by using Eq. (2):

$$k_c = k_B T / < \Delta Z_c^2 > \tag{2}$$

where $< \Delta Z_c^2 >$ is the root mean square of the cantilever beam deformation, which is approximately equal to the area enclosed by the fitted density curve and the horizontal axis, k_B is the Boltzmann constant, and T is the temperature. The obtained values of k_c and InvOLS were substituted into Eq. (1) to complete the calibration.

The PVPA-modified Ti6Al4V was placed in the tank of the AFM system, and the corresponding d value was obtained by loading and unloading the sample (Fig. 6). LiCl, NaCl, KCl, and CsCl were used as lubricants.

PS microspheres were used to apply a force of 10 nN to the PVPA coating, and the force was unloaded after stabilization. During the unloading process, the maximum value of the voltage change was recorded and used as the d value in Eq. (1) to calculate the adhesion between PVPA-modified Ti6Al4V and PS ball in different salt solutions. Furthermore, in order

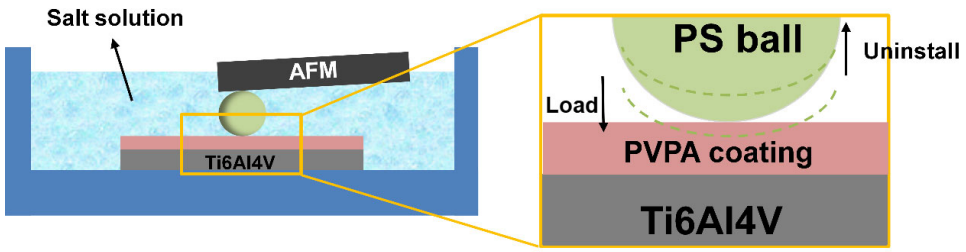

Fig. 6 Schematic diagram of the AFM-submerged experiment measuring the adhesion between PVPA-modified Ti6Al4V and PS ball.

to ensure the accuracy of the experimental results, five repeated experiments were performed for each lubricant, and the average results were obtained, as shown in Fig. 7. When LiCl, NaCl, KCl, and CsCl solutions were used as lubricants, the adhesion forces between PVPA-modified Ti6Al4V and PS ball are 1.00±0.04, 0.86±0.08, 0.72±0.03, and 0.66±0.05 nN, respectively. It was approximated that the size of the cation in the lubricant ($Li^+ < Na^+ < K^+ < Cs^+$) is inversely proportional to the adhesion forces between PVPA-modified Ti6Al4V and PS ball. In other words, the larger the cation, the smaller the adhesion force.

Theoretically, the smaller the adhesion between PVPA-modified Ti6Al4V and PS ball, the smaller the corresponding friction force should be. However, combined with the friction results in Section 3.1, Li^+ is an exception. Relevant study shows that the hydration of ions is an important factor affecting the friction at interface under water lubrication as well. The stronger the hydration, the easier it is to form a hydration layer/membrane. The hydration repulsion provided by the hydration layer will provide a better lubrication effect, thereby reducing the friction coefficient. The smaller the ion size, the greater the corresponding hydration [54]. In this study, the friction force of PVPA surface in salt solution was synergistically regulated by surface adhesion and the hydration of cations. It is speculated that the friction force decreases with the increase of cation size ($\mu_{Na^+} > \mu_{K^+} > \mu_{Cs^+}$) when the effect of surface adhesion on friction force is greater than that of the hydration of cations. When the hydration of cations plays a major role in the friction process, the smaller the cation size, the smaller the corresponding friction force ($\mu_{Li^+} < \mu_{Cs^+}$).

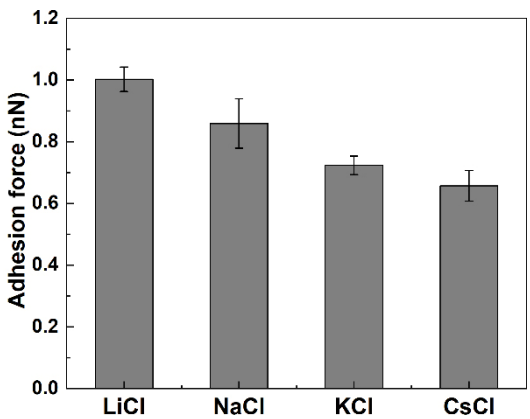

Fig. 7 Adhesion forces between PVPA-modified Ti6Al4V and PS ball in different salt solutions.

3.3 Regulation of cation-induced intermolecular force on PVPA surface adhesion

Relevant studies have shown that the adhesive force F_{ad} of polymer surface is mainly affected by the electrostatic force F_{el}, van der Waals force F_{vdW}, capillary force F_{cap}, and acid–base interaction F_{chem}, represented as Eq. (3):

$$F_{ad} = F_{el} + F_{vdW} + F_{cap} + F_{chem} \tag{3}$$

PVPA was completely immersed in a neutral monovalent salt solution throughout the experiment. It was approximated that the size of F_{cap} was related to air humidity and the hydrophilicity of the interface, while F_{cap} was offset in a liquid environment. Therefore, the influence of F_{cap} on F_{ad} was negligible in this study. In addition, in different friction experiments, only the types of cations in the lubricant were changed, which did not produce obvious chemical transformation differences. So, the influence of F_{chem} on F_{ad} in different friction experiments could also be ignored. In different salt solutions, the difference of PVPA surface adhesion was mainly attributed to the change of F_{vdW} and F_{el} induced by cations.

Next, the MD simulation was used to further analyze the induction difference of F_{vdW} and F_{el} by different cations. Theoretically, the greater the electrostatic energy between the ion and the PVPA molecular chain, the greater the F_{el} between the ion and the PVPA molecular chain. Herein, the Forcite module of Material Studio was used to analyze the interaction between the metal cations and the polymer molecular chains in lubricants. Further, the energy composition of the entire unit cell was analyzed to obtain the electrostatic energy and van der Waals energy between different cations and PVPA molecular chains.

The Amorphous Cell module was used to construct a 3D periodic structure with a unit cell density of 0.8 g/cm^3 and degree of polymerization of 30. One PVPA molecular chain contains 1,000 water molecules and different numbers of inorganic salt ions (Fig. 8).

By employing the energy module, the Ewald method was used to calculate the F_{el}. The atom-based method was used to calculate the F_{vdW}, and a fine cut-off radius (15.5 Å) was selected to calculate the energy of the initial unit cell. Then, based on the Geometry Optimization module, three algorithms, namely the steepest descent method, the conjugate gradient method, and the intelligent method, were used in sequence. Under the conditions of the energy convergence criterion of 0.0001 kcal/(mol·A) and the force convergence criterion of 0.005 kcal/(mol·A), the number of iterations was 50,000, and the global energy composition after structural optimization was obtained (Table 2).

In order to eliminate unnecessary interactions, the model was further calculated by simulated annealing. At temperatures in the range of 300–500 K and the pressure of 0.0001 GPa (1 atm), 10 cycles of annealing

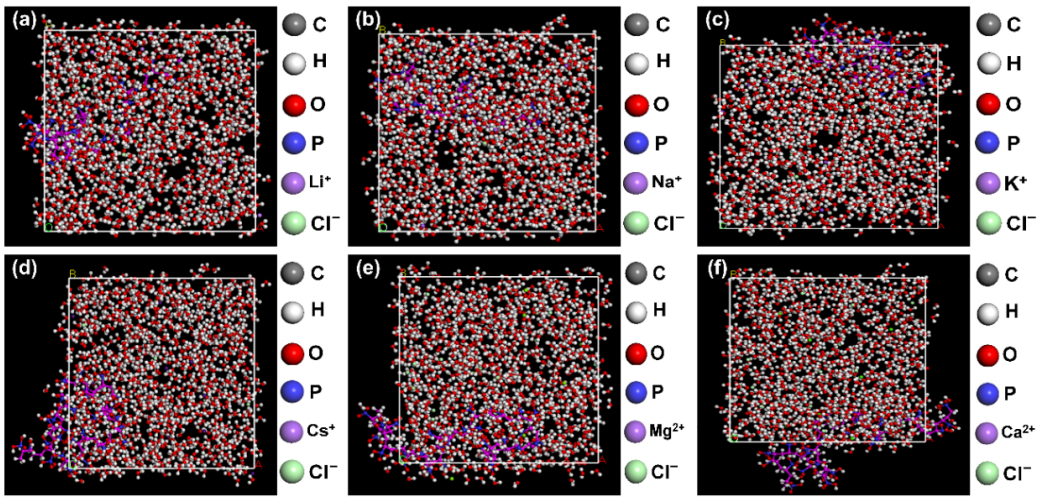

Fig. 8 3D periodic structure models in different inorganic salt solutions: (a) LiCl solution and PVPA, (b) NaCl solution and PVPA, (c) KCl solution and PVPA, (d) CsCl solution and PVPA, (e) $MgCl_2$ solution and PVPA, and (f) $CaCl_2$ solution and PVPA.

Table 2 System energy after structural optimization.

Energy (kcal/mol)	LiCl	NaCl	KCl	CsCl	$MgCl_2$	$CaCl_2$
Total	−14,547.997	−14,293.644	−14,094.148	−13,876.953	−18,210.240	−17,434.515
Non-bond	−16,744.621	−16,462.501	−16,259.124	−16,080.121	−20,418.604	−19,615.099
van der Waals	3,311.099	3,211.057	3,233.423	3,203.135	3,754.426	3,595.323
Electrostatic	−20,041.479	−19,659.352	−19,478.265	−19,269.187	−24,158.614	−23,195.975
Diagonal	2,299.261	2,273.167	2,269.139	2,300.276	2,316.071	2,282.780
Bond	432.428	426.011	426.883	427.704	458.500	439.426
Angle	740.451	691.689	682.177	718.707	716.182	662.603
Torsion	1,126.382	1,155.467	1,160.079	1,153.864	1,141.388	1,180.751
Cross terms	−102.637	−104.310	−104.163	−97.108	−107.706	−102.196

under constant pressure and volume (NPT ensemble) were performed under the condition of 1 fs time step. In each cycle, the temperature was increased from 300 to 500 K in steps of 20 K, and then lowered to 300 K. During the annealing process, the structure further relaxed, and a stable state with minimal local energy was successfully obtained.

Next, after annealing to obtain the overall lowest energy configuration, kinetic simulations under different ensembles were performed. In order to study the interaction between metal cations and polymer molecular chains in different salt solutions, the MD simulation under the NPT ensemble with a pressure of 0.0001 GPa, a temperature of 298 K, a time of 1 fs, and a calculation step of 200,000 was first performed. After reaching the initial equilibrium state, the MD simulation was performed in the NVT ensemble with a temperature of 298 K, a calculation time step of 1 fs, and a calculation step of 200,000. After the completion of the simulation, the temperature was found to fluctuate within a certain period, and then it stabilized within 5%–6% and reached a constant temperature. Moreover, the energy of different unit cells fluctuated around a relatively fixed value. The temperature and energy of different unit cells changed with time are shown in Fig. 9. Therefore, it could be speculated that each unit cell could reach an equilibrium after the completion of the kinetic simulation. The ordinate values were gradually shifted upwards by 20 from the second line, as shown in Fig. 9(a), illustrating a stark contrast.

During the MD simulation process, the Ewald method was used to calculate the F_{el}, the F_{vdW} was calculated based on the atom method, and a fine cut-off radius (15.5 Å) was selected. In the unit cell, a Nose thermostat was used to control the temperature in order to further obtain the global minimum energy (Table 3).

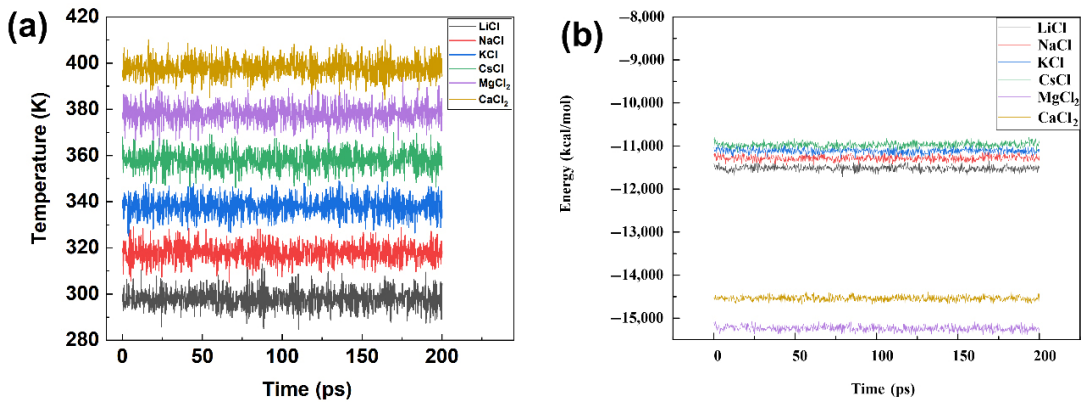

Fig. 9 Changes in temperature and energy of different unit cells over time: (a) temperature–time fluctuation diagram of different unit cells; (b) energy–time fluctuation diagram of different unit cells.

Table 3 Unit cell energy and its composition after kinetic simulation.

Energy (kcal/mol)	LiCl	NaCl	KCl	CsCl	$MgCl_2$	$CaCl_2$
Total	−8,565.716	−8,524.941	−8,124.966	−7,993.097	−12,266.522	−11,414.153
Non-bond	−14,835.646	−14,688.913	−14,288.305	−14,269.198	−18,564.440	−17,720.872
van der Waals	2,757.589	2,747.675	2,586.846	2,644.576	3,272.731	3,105.799
Electrostatic	−17,593.235	−17,436.588	−16,913.774	−16,875.151	−21,837.172	−20,826.671
Diagonal	3,467.417	3,387.705	3,327.237	3,453.337	3,439.889	3,320.909
Bond	1,212.381	1,152.816	1,111.018	1,205.013	1,196.025	1,173.064
Angle	1,134.625	1,102.936	1,095.659	1,123.500	1,120.452	1,019.540
Torsion	1,120.412	1,131.954	1,120.560	1,124.825	1,123.412	1,128.305
Cross terms	−104.826	−107.478	−105.400	−105.590	−110.689	−103.953
Density (g/cm^3)	1.044	1.039	1.060	1.078	1.054	1.057

Tables 2 and 3 summarize that comparative analysis based on the optimized unit cell energy indicates that the energy of each unit cell after annealing and kinetics simulation is reduced significantly to a lower value. Therefore, in the following dynamic simulation, the unit cell reached the equilibrium very easily.

In order to more intuitively compare the energy between different unit cells, the total energy and electrostatic interaction energy of the unit cell after kinetic simulation were analyzed, as shown in Fig. 10. The average value of total energy and electrostatic energy of different cations has been calculated by at least four simulation results. By changing different lubricant types, in the overall energy composition of each unit cell, non-bonding energy has always been the most important part of the energy of the entire unit cell, accounting for about 55%–70% of the total. Among them, the electrostatic interaction energy between the inorganic phase and the organic phase is the main component of the non-bonding energy, accounting for about 80%. The difference from the above-mentioned phenomenon is that even if the type of lubricant changes, the van der Waals energy between different unit cells is not significantly different, and thus the influence of F_{vdW} on the interaction between different metal cations and PVPA molecular chains can be ignored.

For monovalent metal cations, with the increase in the radius of the cation ($Li^+ < Na^+ < K^+ < Cs^+$), the electrostatic interaction energy between the cation and the PVPA molecular chain decreases. In order to verify the universality of this law, the above-mentioned simulations were performed using $MgCl_2$ and $CaCl_2$ as lubricants, and the corresponding results are shown in Figs. 8–10. The corresponding energy and composition after structural optimization and the MD simulation were obtained, and the values are listed in Tables 2 and 3, respectively. For divalent cations, the larger the ionic radius, the smaller the electrostatic interaction energy of the ion present on the molecular chains. Therefore, consequently, for metal cations with the same valence state, the larger the ionic radius, the smaller the electrostatic interaction energy between the ion and the polymer molecular chain, and the smaller the corresponding electrostatic force. In conclusion, combined analysis of the adhesion forces between PVPA-modified Ti6Al4V and PS ball by AFM indicates that the smaller the electrostatic force between the metal cation and the surface of PVPA, the smaller the corresponding adhesion between the surfaces. Noteworthy, by controlling the ionic radius, the electrostatic force between the ions and the PVPA surface can be indirectly adjusted, and thus finally the purpose of adjusting the adhesion force is achieved.

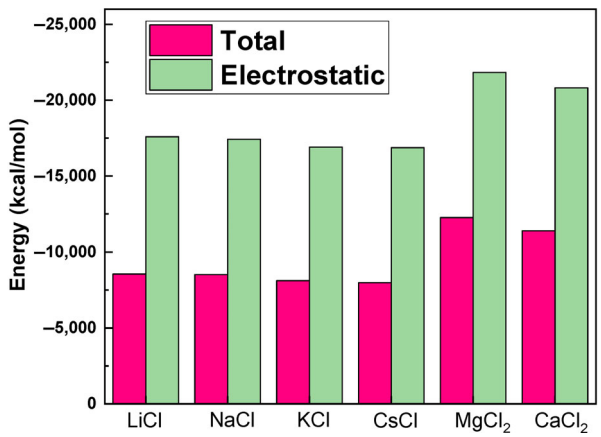

Fig. 10 Total energy of the unit cell and its electrostatic interaction energy after kinetic simulation.

The existence of alkali metal cations in the lubricant would change the electrostatic energy of the entire tribo-systems, thereby reducing the adhesion force between the PVPA coating and the PS microsphere probe. On this basis, the resultant force of the normal force and the frictional force on the surface of the PVPA coating were also reduced, so that the friction coefficient of the PVPA surface was extremely low, so the superlubricity was realized in the friction process. It was worth noting that the ionic radius was an important factor affecting adhesion and friction. For monovalent salt ions, the larger the ion radius ($Na^+ < K^+ < Cs^+$), the smaller the electrostatic force, and the smaller the adhesion force, so that the friction coefficient gradually decreased on the basis of superlubricity.

4 Conclusions

The effects of metal cations present in salt solution on the friction properties of PVPA molecular chains were studied by the AFM and MD simulation. Interestingly, the PVPA coating achieves superlubricity

under the lubrication condition of monovalent salt solution. The friction of the PVPA surface is co-regulated by surface adhesion and hydration of cations. The friction decreases with the increase of cation size when the effect of surface adhesion on friction is larger than the hydration of cations. Conversely, friction decreases with the decrease of cation size. From the perspective of intermolecular forces, the electrostatic force is the main factor affecting the change in surface friction characteristics of PVPA. Simulation results show that with the increase of salt ionic radius ($Li^+ < Na^+ < K^+ < Cs^+$), the electrostatic interaction energy between cation and PVPA molecular chain decreases. Furthermore, when divalent metal cations are introduced for comparative analysis, the same phenomenon as that of monovalent cations is also successfully achieved. It thus shows that the difference of electrostatic interaction between metal cation and PVPA molecular chain obtained under experimental conditions is related to the difference of frictional characteristic on PVPA surface. Therefore, by adjusting the size of the cation radius in the lubricant, the adhesion force between PVPA-modified Ti6Al4V and PS microspheres can be changed, and thus affects the magnitude of friction between the tribological pairs. The influence of intermolecular forces induced by different metal cations on the tribological properties of PVPA coatings is of guiding significance for the further study of superlubricity of hydrophilic polymers.

Acknowledgements

This work was supported by the National Natural Science Foundation of China (51705010), the Beijing Natural Science Foundation (3192003), the General Project of Science and Technology Plan from Beijing Educational Committee (KM201810005013), the Tribology Science Fund of State Key Laboratory of Tribology (STLEKF16A02 and SKLTKF19B08), and the training program of Rixin talent and outstanding talent from Beijing University of Technology.

References

[1] Keum H, Kim J Y, Yu B, Yu S J, Kim J, Jeon H, Lee D Y, Im S G, Jon S. Prevention of bacterial colonization on catheters by a one-step coating process involving an antibiofouling polymer in water. *ACS Appl Mater Interfaces* **9**(23): 19736–19745 (2017)

[2] Ran B, Jing C Y, Yang C, Li X N, Li Y H. Synthesis of efficient bacterial adhesion-resistant coatings by one-step polydopamine-assisted deposition of branched polyethylenimine-g-poly(sulfobetaine methacrylate) copolymers. *Appl Surf Sci* **450**: 77–84 (2018)

[3] Woo J, Seo H, Na Y, Choi S, Kim S, Choi W I, Park M H, Sung D. Facile synthesis and coating of aqueous antifouling polymers for inhibiting pathogenic bacterial adhesion on medical devices. *Prog Org Coat* **147**: 105772 (2020)

[4] Oh Y J, Khan E S, Campo A D, Hinterdorfer P, Li B. Nanoscale characteristics and antimicrobial properties of (SI-ATRP)-seeded polymer brush surfaces. *ACS Appl Mater Interfaces* **11**(32): 29312–29319 (2019)

[5] Rodriguez-Emmenegger C, Janel S, de los Santos Pereira A, Bruns M, Lafont F. Quantifying bacterial adhesion on antifouling polymer brushes via single-cell force spectroscopy. *Polym Chem* **6**(31): 5740–5751 (2015)

[6] Kusunoki T, Oshiro M, Hamasaki F, Kobayashi T. Polyvinylphosphonic acid copolymer hydrogels prepared with amide and ester type crosslinkers. *J Appl Polym Sci* **119**(5): 3072–3079 (2011)

[7] Franco R A, Sadiasa A, Lee B T. Utilization of PVPA and its effect on the material properties and biocompatibility of PVA electrospun membrane. *Polym Adv Technol* **25**(1): 55–65 (2014)

[8] Han S Y, Yue B H, Yan L M. Improving the performances of poly(vinylphosphonic acid) by compositing or copolymerization with poly(4-(α-methyl)vinyl-1H-1,2,3-triazole). *Electrochimica Acta* **138**: 256–263 (2014)

[9] Nooralian Z, Parvinzadeh Gashti M, Ebrahimi I. Fabrication of a multifunctional graphene/polyvinylphosphonic acid/cotton nanocomposite via facile spray layer-by-layer assembly. *RSC Adv* **6**(28): 23288–23299 (2016)

[10] Bozkurt A, Ling X, Domke K F. Proton conductivity and structural properties of nanocomposites based on boehmite incorporated poly(vinlyphosphonic acid). *Ionics* **25**(10): 4831–4840 (2019)

[11] Zhang C X, Liu Z F, Liu Y H, Cheng Q, Yang C B, Cai L G. Investigation of the mechanisms for stable superlubricity of poly(vinylphosphonic acid) (PVPA) coatings affected by lubricant. *Friction* **4**(4): 303–312 (2016)

[12] Luo J B, Zhou X. Superlubricitive engineering—Future industry nearly getting rid of wear and frictional energy consumption. *Friction* **8**(4): 643–665 (2020)

[13] Zhang C X, Chen J M, Liu M M, Liu Y H, Liu Z F, Chu H Y, Cheng Q, Wang J H. Regulation mechanism of biomolecule interaction behaviors on the superlubricity of hydrophilic polymer coatings. *Friction* **10**(1): 94–109 (2022)

[14] Liu Z F, Liu M M, Liu Y, Zhang C X, Wang X Z, Ma L R, Cai H Y, Cheng Q. Molecular arrangement mechanisms within phosphate films on Ti6Al4V regulated by intermolecular forces based on sum frequency generation vibrational spectroscopy. *Appl Surf Sci* **521**: 146364 (2020)

[15] Zhang C X, Liu Z F, Liu Y H, Ren J, Cheng Q, Yang C B, Cai L G. Novel tribological stability of the superlubricity poly(vinylphosphonic acid) (PVPA) coatings on Ti6Al4V: Velocity and load independence. *Appl Surf Sci* **392**: 19–26 (2017)

[16] Ren Y L, Zhang L, Xie G X, Li Z B, Chen H, Gong H J, Xu W H, Guo D, Luo J B. A review on tribology of polymer composite coatings. *Friction* **9**(3): 429–470 (2021)

[17] Zhang Y P, Li P P, Ji L, Liu X H, Wan H Q, Chen L, Li H X, Jin Z L. Tribological properties of MoS_2 coating for ultra-long wear-life and low coefficient of friction combined with additive g-C_3N_4 in air. *Friction* **9**(4): 789–801 (2021)

[18] Zhang R J, Shi W X, Yu S L, Wang W, Zhang Z Q, Zhang B, Li L, Bao X. Influence of salts, anion polyacrylamide and crude oil on nanofiltration membrane fouling during desalination process of polymer flooding produced water. *Desalination* **373**: 27–37 (2015)

[19] Lu J, Qin Y Y, Zhang Q, Wu Y L, Cui J Y, Li C X, Wang L, Yan Y S. Multilayered ion-imprinted membranes with high selectivity towards Li^+ based on the synergistic effect of 12-crown-4 and polyether sulfone. *Appl Surf Sci* **427**: 931–941 (2018)

[20] Liu X J, Ye Q, Yu B, Liang Y M, Liu W M, Zhou F. Switching water droplet adhesion using responsive polymer brushes. *Langmuir* **26**(14): 12377–12382 (2010)

[21] Mallinson D, Mullen A B, Lamprou D A. Probing polydopamine adhesion to protein and polymer films: Microscopic and spectroscopic evaluation. *J Mater Sci* **53**(5): 3198–3209 (2018)

[22] Et-Thakafy O, Delorme N, Gaillard C, Mériadec C, Artzner F, Lopez C, Guyomarc'h F. Mechanical properties of membranes composed of gel-phase or fluid-phase phospholipids probed on liposomes by atomic force spectroscopy. *Langmuir* **33**(21): 5117–5126 (2017)

[23] Füllbrandt M, Kesal D, von Klitzing R. Multiscaling approach for non-destructive adhesion studies of metal/polymer composites. *ACS Appl Mater Interfaces* **7**(30): 16247–16256 (2015)

[24] Picas L, Milhiet P E, Hernández-Borrell J. Atomic force microscopy: A versatile tool to probe the physical and chemical properties of supported membranes at the nanoscale. *Chem Phys Lipids* **165**(8): 845–860 (2012)

[25] Wang X, Wong S C, Jung Y J, Wan K T. Measuring interfacial adhesion of carbon nanotube bundles and electrospun polymer fibers. *Langmuir* **33**(44): 12592–12595 (2017)

[26] Zhang L, Ren Y L, Peng S G, Guo D, Wen S Z, Luo J B, Xie G X. Core–shell nanospheres to achieve ultralow friction polymer nanocomposites with superior mechanical properties. *Nanoscale* **11**(17): 8237–8246 (2019)

[27] Bilotto P, Labate C, de Santo M P, Deepankumar K, Miserez A, Zappone B. Adhesive properties of adsorbed layers of two recombinant mussel foot proteins with different levels of DOPA and tyrosine. *Langmuir* **35**(48): 15481–15490 (2019)

[28] Moradi M, Fereidon A H, Sadeghzadeh S. Aspect ratio and dimension effects on nanorod manipulation by atomic force microscope. *Micro Nano Lett* **5**(5): 324–327 (2010)

[29] Zhang X L, Lu Y J, Liu E Y, Yi G W, Jia J H. Adhesion and friction studies of microsphere-patterned surfaces in contact with atomic force microscopy colloidal probe. *Colloids Surf A Physicochem Eng Aspects* **401**: 90–96 (2012)

[30] Ducker W A, Senden T J, Pashley R M. Direct measurement of colloidal forces using an atomic force microscope. *Nature* **353**(6341): 239–241 (1991)

[31] Abhyankar H, Webb D P, West G D, Hutt D A. Characterization of metal–polymer interaction forces by AFM for insert molding applications. *Polym Eng Sci* **60**(12): 3036–3045 (2020)

[32] Duan Y Q, Liu Y H, Zhang C X, Chen Z, Wen S Z. Insight into the tribological behavior of liposomes in artificial joints. *Langmuir* **32**(42): 10957–10966 (2016)

[33] Duan Y Q, Liu Y H, Li J J, Wang H D, Wen S Z. Investigation on the nanomechanics of liposome adsorption on titanium alloys: Temperature and loading effects. *Polymers* **10**(4): 383 (2018)

[34] Laitinen O, Bauer K, Niinimäki J, Peuker U A. Validity of the Rumpf and the Rabinovich adhesion force models for alumina substrates with nanoscale roughness. *Powder Technol* **246**: 545–552 (2013)

[35] Yao N Q, Wang H B, Zhang L Q, Yue D M, Tian M. One-pot solvothermal synthesis of silane-functionalized carbon nanodots as compatibilizers for the immiscible TPU/MVQ blends. *Appl Surf Sci* **530**: 147124 (2020)

[36] Çolak A, Wormeester H, Zandvliet H J W, Poelsema B. Surface adhesion and its dependence on surface roughness and humidity measured with a flat tip. *Appl Surf Sci* **258**(18): 6938–6942 (2012)

[37] Riley J K, Matyjaszewski K, Tilton R D. Friction and adhesion control between adsorbed layers of polyelectrolyte brush-grafted nanoparticles via pH-triggered bridging interactions. *J Colloid Interface Sci* **526**: 114–123 (2018)

[38] Ishak M I, Dobryden I, Martin Claesson P, Briscoe W H, Su B. Friction at nanopillared polymer surfaces beyond Amontons' laws: Stick–slip amplitude coefficient (SSAC) and multiparametric nanotribological properties. *J Colloid Interface Sci* **583**: 414–424 (2021)

[39] Michałowski M, Łuczak S. AFM cantilevers with spherical tip of millimeter size. *J Micromech Microeng* **29**(1): 017002 (2019)

[40] An J X, Jin C S, Dėdinaitė A, Holgersson J, Karlsson N G, Claesson P M. Influence of glycosylation on interfacial properties of recombinant mucins: Adsorption, surface forces, and friction. *Langmuir* **33**(18): 4386–4395 (2017)

[41] Dehghani E S, Ramakrishna S N, Spencer N D, Benetti E M. Engineering lubricious, biopassive polymer brushes by surface-initiated, controlled radical polymerization. *Ind Eng Chem Res* **57**(13): 4600–4606 (2018)

[42] Dehghani E S, Ramakrishna S N, Spencer N D, Benetti E M. Controlled crosslinking is a tool to precisely modulate the nanomechanical and nanotribological properties of polymer brushes. *Macromolecules* **50**(7): 2932–2941 (2017)

[43] Raftari M, Zhang Z J, Carter S R, Leggett G J, Geoghegan M. Nanoscale contact mechanics between two grafted polyelectrolyte surfaces. *Macromolecules* **48**(17): 6272–6279 (2015)

[44] Hanson B, Hofmann J, Pasquinelli M A. Influence of copolyester composition on adhesion to soda-lime glass via molecular dynamics simulations. *ACS Appl Mater Interfaces* **8**(21): 13583–13589 (2016)

[45] Zhang L, Xie G X, Wu S, Peng S G, Zhang X Q, Guo D, Wen S Z, Luo J B. Ultralow friction polymer composites incorporated with monodispersed oil microcapsules. *Friction* **9**(1): 29–40 (2021)

[46] Wu Z T, Zhou J J. Mechanical properties of interlocked-ring polymers: A molecular dynamics simulation study. *Chin J Polym Sci* **37**(12): 1298–1304 (2019)

[47] Song J F, Zhao G. A molecular dynamics study on water lubrication of PTFE sliding against copper. *Tribol Int* **136**: 234–239 (2019)

[48] Sun X Y, Qi Y Z, Ouyang W G, Feng X Q, Li Q Y. Energy corrugation in atomic-scale friction on graphite revisited by molecular dynamics simulations. *Acta Mech Sin* **32**(4): 604–610 (2016)

[49] Hu C Z, Bai M L, Lv J Z, Wang P, Li X J. Molecular dynamics simulation on the friction properties of nanofluids confined by idealized surfaces. *Tribol Int* **78**: 152–159 (2014)

[50] Dai L, Sorkin V, Zhang Y W. Probing the surface profile and friction behavior of heterogeneous polymers: A molecular dynamics study. *Model Simul Mater Sci Eng* **25**(3): 035003 (2017)

[51] Wang W, Xie G X, Luo J B. Superlubricity of black phosphorus as lubricant additive. *ACS Appl Mater Interfaces* **10**(49): 43203–43210 (2018)

[52] Kim K, Ghosh A, Lee K S, Lee W B. Molecular dynamics study of the role of friction on the thermal rupture of linear alternate copolymers. *Macromol Res* **19**(11): 1192–1194 (2011)

[53] He E Q, Wang S J, Li Y L, Wang Q. Enhanced tribological properties of polymer composites by incorporation of nano-SiO_2 particles: A molecular dynamics simulation study. *Comput Mater Sci* **134**: 93–99 (2017)

[54] Gaisinskaya-Kipnis A, Ma L R, Kampf N, Klein J. Frictional dissipation pathways mediated by hydrated alkali metal ions. *Langmuir* **32**(19): 4755–4764 (2016)

Hongyun CAI. He received his bachelor degree from Anhui Agricultural University, China, in 2018. He is currently a graduate student at Institute of Advanced Manufacturing and Intelligent Technology, Beijing University of Technology, China. His research interests include nanotribology and molecular dynamics simulation.

Caixia ZHANG. She received her Ph.D. degree in mechanical engineering from Tsinghua University, China, in 2015. After then, she joined Beijing Key Laboratory of Advanced Manufacturing Technology, Beijing University of Technology, China. Her research interests include biotribology, superlubricity, surface and interface analysis.

Fuping LI. She received her master degree in mechanical from South China University of Technology, China, in 1998. She currently works in Institute of Advanced Manufacturing and Intelligent Technology, Beijing University of Technology, China. Her research interests include digital manufacturing and friction.

Mengmeng LIU. She received her bachelor degree from Applied Technology College of Soochow University, China. She is currently a graduate student at the Beijing University of Technology, China. Her research interests include superlubricity and control of smart surface and interface.

Tao ZHANG. He received his Ph.D. degrees from Beijing University of Technology, China, in 2020. He is currently a research assistant in the Institute of Advanced Manufacturing and Intelligent Technology, Beijing University of Technology. His research interests include optimization design and meshing characteristics analysis of harmonic drive, surface and interface analysis.

Hongyan CHU. She received her Ph.D. degree in mechanical design and theory from Beijing University of Technology, China, in 2003. And she currently works in Institute of Advanced Manufacturing and Intelligent Technology, Beijing University of Technology. Her research interests include intelligent manufacturing technology, surface and friction characteristics, and contact dynamics of viscoelastic material.

Zhifeng LIU. He received his Ph.D. degree in mechanical engineering from Northeastern University, China. He is the team leader of the Institute of Advanced Manufacturing and Intelligent Technology, Beijing University of Technology and Key Laboratory of CNC Equipment Reliability, Ministry of Education, Jilin University. His research interests include heavy-duty machine tool, superlubricity, robot, and assembly technology.